

Supporting Information: Ru/Rh Catalyzed Selective Hydrogenation of CO₂ to Formic Acid: A First Principles Microkinetic Analysis

Sourav Ghoshal,[†] Prodyut Roy,[†] Anup Pramanik,[‡] and Pranab Sarkar^{*,†}

*Department of Chemistry, Visva-Bharati University, Santiniketan- 731235, India, and Department
of Chemistry, Purulia- 723104, India*

E-mail: pranab.sarkar@visva-bharati.ac.in

*To whom correspondence should be addressed

[†]Visva-Bharati University

[‡]Sidho-Kanho-Birsha University

S1 Microkinetic Modeling

All microkinetic simulations were performed by using the MKMCXX program, based on mean-field microkinetic modeling (MKM).¹⁻³ The kinetics of the entire reaction network were used to calculate by assuming the quasi-equilibrium approximation, in which all steps other than the rate-determining step are in quasi-equilibrium. Using these approximations, one can obtain the surface coverage (θ) of various species and overall reaction rate (s^{-1}). A typical catalytic reaction has three important steps: adsorption, desorption and surface reactions. On the basis of statistical thermodynamics, the rate constant of any elementary reaction step can be calculated by following general equation:

$$k = \frac{k_b T}{h} \frac{Q_{TS}^\ddagger}{Q_{IS}} \exp\left(-\frac{\Delta E_0}{k_b T}\right) \quad (1)$$

In Eq. (1), Q_{TS} , Q_{IS} , ΔE_0 , k_b and h are the symbols for partition functions of the transition state, initial state (pre-reactive complex), energy change of elementary step, Boltzmann and Planck constants, respectively.

The rate constants of adsorption and desorption steps were derived by employing Hertz-Knudsen kinetics.⁴ For the non-activated adsorption step ($E_0 = 0$), the Eq. (1) can be simplified as:

$$k_{ads} = \frac{PA}{\sqrt{2\pi m k_b T}} S \quad (2)$$

Here, k_{ads} , P , A , m and S denote adsorption rate constant, partial pressure of the molecule in the gas phase, effective surface area of the catalyst, mass of the adsorbate and sticking coefficient, respectively. The sticking coefficient used here is 1 for CO_2 and H_2 adsorptions. The above expression was derived by assuming following assumptions that the transition state is a loose transition state, molecule loses one translational degree of freedom during migration from the gas phase to the catalyst surface, ideal gas law is valid, changes in the rotational degrees of freedom is negligible and vibrational degrees of freedom is unity under typical reaction conditions.

For the desorption step, which is just opposite to the adsorption, the transition state has three

rotational degrees of freedom and two translational degrees of freedom, however, as molecule leaves from catalyst surface to gas phase, therefore it was assumed that initial state (surface bound adsorbed state) only contains vibrational degrees of freedom. Accordingly, the rate constant for the desorption process can be expressed as:

$$k_{des} = \frac{k_b T^3}{h^3} \frac{A(2\pi m k_b)}{\sigma \Theta_{rot}} \exp\left(-\frac{E_{des}}{k_B T}\right) \quad (3)$$

In Eq. (3), σ , Θ_{rot} and E_{des} are the symmetry number, characteristic temperature for rotation and desorption energy, respectively.

The rate constants for the forward and backward elementary reactions were determined by the Eyring equation:⁵

$$k = A(T) \exp\left(-\frac{E_a}{k_b T}\right) \quad (4)$$

In Eq. (4), E_a is the reaction barrier, which is the zero point energy corrected electronic energy difference between initial and transition state. The pre-exponential factor (A) is calculated from the entropy change between initial and transition state of the first-order elementary step, which can be expressed as:

$$A(T) = \frac{k_b T}{h} \frac{Q_{TS}^\ddagger}{Q_{IS}} \quad (5)$$

Notably, catalytic surface typically only have vibrational degrees of freedom, partition function (vibrational) ratios equal almost to unity, and thus pre-factor was roughly estimated in the order of 10^{13} in many previous works.⁶⁻⁹ For the present MKM simulations, we have calculated partition function ratio between the transition state and initial state, as presented in Tables S9 to S11.

A set of ordinary differential equations (ODEs) are constructed using the rate constants of elementary reaction steps. By using the appropriate initial conditions and model parameters, the MKMCXX can solve this set of ODEs by means of the Backward Differentiation Formula (BDF) method.² BDF is commonly used to solve stiff differential equations. Steady-state coverages are also calculated by integrating the ODEs over time, until the changes in the surface coverages were very small. The rates of individual elementary steps and overall reaction can be computed on

the basis of steady-state surface coverages. The degree of rate control (DRC) calculation was also performed to identify which elementary step contribute mostly to the rate control over the overall reaction. The method introduced by the Campbell and coworkers,¹⁰ were employed for this purpose. For the elementary step *i*, the degree of rate control (χ_i) is defined as:

$$\chi_i = \frac{k_i}{r} \left(\frac{\partial r}{\partial k_i} \right)_{k_j \neq k_i, K_i} = \left(\frac{\partial \ln r}{\partial \ln k_i} \right)_{k_j \neq k_i, K_i} \quad (6)$$

In Eq. (6), k_i , K_i and r are the rate constants, the equilibrium constant for step *i* and the reaction rate, respectively. A positive value of χ_i indicates the reaction step is rate controlling and negative value means the step is rate inhibiting. Larger the the value of χ_i , for a given step, the greater its contribution to the overall reaction rate.

Table (S1) Relative energy of the lowest energy ruthenium conformers (Ru_x) between different spin states (M_s (E)) in kcal/mol. Here, L1 and L2 stand for BLYP and B3LYP level of theories.

Ru_x	Level's	M_s (E)				
$x = 4$	L1	1 (0.0)	3 (6.5)	5 (4.0)	7 (7.3)	9 (5.6)
	L2	3 (15.7)	5 (15.1)	7 (12.5)	9 (0.0)	11 (7.4)
$x = 5$	L1	1 (0.0)	3 (1.7)	5 (8.5)	7 (9.8)	9 (12.2)
	L2	9 (12.5)	11 (7.5)	13 (1.7)	15 (0.0)	17 (7.0)
$x = 6$	L1	1 (2.3)	3 (1.6)	5 (0.0)	7 (8.0)	9 (11.6)
	L2	9 (12.8)	11 (15.3)	13 (17.4)	15 (0.0)	17 (5.5)
$x = 7$	L1	1 (2.6)	3 (2.9)	5 (0.0)	7 (3.2)	9 (8.4)
$x = 8$	L1	1 (1.8)	3 (1.3)	5 (0.0)	7 (8.9)	9 (22.2)

Table (S2) Relative energy of the lowest energy CO_2 adsorbed ruthenium conformers (Ru_xCO_2) between different spin states (M_s (E)) in kcal/mol. Here, L1 and L2 stand for BLYP and B3LYP level of theories.

Ru_xCO_2	Level's	M_s (E)				
$x = 4$	L1	1 (0.0)	3 (2.1)	5 (2.4)	7 (3.5)	9 (12.3)
	L2	3 (14.0)	5 (19.7)	7 (12.0)	9 (11.8)	11 (0.0)
$x = 5$	L1	1 (0.0)	3 (2.7)	5 (7.0)	7 (10.9)	9 (12.2)
	L2	9 (3.2)	11 (0.0)	13 (0.8)	15 (17.2)	17 (22.6)
$x = 6$	L1	1 (1.2)	3 (0.0)	5 (0.1)	7 (5.4)	9 (11.0)
	L2	7 (1.9)	9 (3.4)	11 (7.1)	13 (0.0)	15 (1.2)
$x = 7$	L1	1 (1.1)	3 (0.0)	5 (1.6)	7 (3.2)	9 (10.1)
$x = 8$	L1	1 (2.5)	3 (2.9)	5 (0.0)	7 (10.3)	9 (23.6)

Table (S3) Relative energy of the lowest energy rhodium conformers (Rh_x) between different spin states (M_s (E)) in kcal/mol. Here, L1 and L2 stand for BLYP and B3LYP level of theories.

Rh_x	Level's	M_s (E)				
$x = 4$	L1	1 (0.0)	3 (5.0)	5 (3.3)	7 (4.0)	9 (11.2)
	L2	1 (7.9)	3 (10.3)	5 (8.3)	7 (0.0)	9 (17.1)
$x = 5$	L1	2 (6.2)	4 (2.9)	6 (0.7)	8 (0.0)	10 (9.9)
	L2	2 (9.8)	4 (5.4)	6 (0.0)	8 (0.0)	10 (2.1)
$x = 6$	L1	1 (7.6)	3 (6.9)	5 (5.2)	7 (0.0)	9 (2.6)
	L2	5 (8.9)	7 (0.0)	9 (3.0)	11 (5.3)	13 (14.4)
$x = 7$	L1	6 (9.0)	8 (4.8)	10 (0.2)	12 (0.0)	14 (2.3)
$x = 8$	L1	5 (14.4)	7 (10.6)	9 (9.1)	11 (5.4)	13 (0.0)

Table (S4) Relative energy of the lowest energy CO_2 adsorbed rhodium conformers (Rh_xCO_2) between different spin states (M_s (E)) in kcal/mol. Here, L1 and L2 stand for BLYP and B3LYP level of theories.

Rh_xCO_2	Level's	M_s (E)				
$x = 4$	L1	1 (5.7)	3 (3.3)	5 (4.1)	7 (0.0)	9 (22.9)
	L2	1 (7.9)	3 (10.3)	5 (8.3)	7 (0.0)	9 (17.1)
$x = 5$	L1	2 (5.8)	4 (3.3)	6 (0.9)	8 (0.0)	10 (16.7)
	L2	2 (9.8)	4 (5.4)	6 (0.0)	8 (0.0)	10 (2.1)
$x = 6$	L1	1 (5.5)	3 (3.8)	5 (1.9)	7 (0.0)	9 (0.0)
	L2	5 (8.9)	7 (0.0)	9 (3.0)	11 (5.3)	13 (14.4)
$x = 7$	L1	6 (4.0)	8 (0.5)	10 (0.0)	12 (1.8)	14 (11.2)
$x = 8$	L1	5 (6.6)	7 (3.5)	9 (2.1)	11 (0.0)	13 (3.9)

Table (S5) Energies (eV) of supported catalysts at different force threshold (EDIFFG).

Catalysts	-0.05 eV/Å	-0.025 eV/Å
$\text{Ru}_2@ \text{TiO}_2(\text{v})$	-565.19626581	-565.19711864
$\text{Rh}_2@ \text{TiO}_2(\text{v})$	-557.09556539	-557.09433110
$\text{Ru}_4@ \text{TiO}_2(\text{v})$	-769.38183782	-769.38243006
$\text{Rh}_4@ \text{TiO}_2(\text{v})$	-753.17874020	-753.17915548

Table (S6) Calculated vibrational frequencies, zero point energies (ZPE) and entropy (TS) of different intermediates and transition states on supported dimers for RWGS pathway, where the * denotes the adsorption site.

Ru ₂ @TiO ₂ (v)	(CO ₂ *) ₁ +2H*	T_S-1	COOH*+H*	T_S-2	CO*+OH*+H*	T_S-3	CO*+H ₂ O*
Freq (cm ⁻¹)	3605.80	3256.46	3619.76	3640.76	3686.64	3649.84	3767.75
	2149.27	1883.24	2870.45	2842.76	2669.82	2371.48	3658.74
	1435.34	1585.05	1657.49	1653.31	1536.97	1453.38	1579.76
	1293.30	1270.68	1303.89	1396.76	1451.82	1266.97	1509.73
	1095.75	998.13	1000.58	818.61	765.69	843.13	557.20
	735.50	788.18	695.35	649.74	604.24	566.66	504.55
	722.99	704.58	638.49	583.44	568.21	523.63	445.32
	685.94	547.91	622.30	536.62	549.08	508.76	414.62
	518.06	512.34	517.42	494.17	513.51	496.05	350.07
	443.33	432.34	482.39	453.99	495.71	432.71	260.22
	382.94	368.06	400.52	431.06	316.77	307.64	211.62
	357.64	301.90	342.89	302.13	304.20	252.47	180.12
	309.92	244.43	260.61	258.73	252.63	161.57	169.11
	231.16	221.95	233.93	172.48	119.30	120.85	40.94
	193.50	1224.02 (i)	220.71	243.21 (i)	101.10	840.57 (i)	24.52
ZPE (eV)	0.88	0.81	0.92	0.88	0.86	0.80	0.85
TS (eV)	0.13	0.12	0.13	0.12	0.18	0.16	0.29
Rh ₂ @TiO ₂ (v)	(CO ₂ *) ₁ +2H*	T_S-1	COOH*+H*	T_S-2	CO*+OH*+H*	T_S-3	CO*+H ₂ O*
Freq (cm ⁻¹)	3074.08	1837.47	3573.51	3672.04	3707.74	3707.63	3735.00
	1473.62	1642.34	1865.59	1819.76	2037.78	1999.26	3632.80
	1384.64	1262.19	1291.55	1453.08	1479.59	1500.36	1738.66
	1104.96	997.00	1121.31	877.41	849.07	925.97	1577.87
	882.27	879.26	839.00	660.54	654.96	689.87	610.74
	744.86	720.57	715.84	599.31	591.05	558.39	541.24
	516.60	592.06	670.48	560.07	546.82	524.19	527.78
	490.66	452.21	626.24	494.47	519.39	504.39	481.89
	422.59	434.57	547.63	480.62	494.76	448.32	408.22
	375.45	368.14	378.86	434.70	446.54	303.13	321.39
	351.81	306.66	354.58	370.17	308.58	282.00	202.98
	296.54	283.71	288.97	294.61	261.81	235.52	194.83
	285.37	244.12	265.22	252.91	229.08	121.86	116.13
	227.80	216.56	247.86	149.54	120.02	96.77	88.08
	205.89	1448.68 (i)	193.25	201.06 (i)	93.62	890.62 (i)	4.32
ZPE (eV)	0.73	0.63	0.80	0.75	0.77	0.74	0.88
TS (eV)	0.15	0.13	0.14	0.14	0.20	0.19	0.20

Table (S7) Calculated vibrational frequencies, zero point energies (ZPE) and entropy (TS) of different intermediates and transition states on supported dimers for formic acid formation reaction, where the * denotes the adsorption site.

Ru ₂ @TiO ₂ (v)	(CO ₂ *) ₂ +2H*	T_S-4	HCOO*+H*	T_S-5	HCOOH*
Freq (cm ⁻¹)	2022.67	2159.78	3514.13	2844.34	3304.34
	1682.03	1827.15	3008.65	1280.40	2867.53
	1399.71	1386.96	1500.56	1239.09	1295.28
	1184.99	1164.25	1348.71	1155.73	1255.60
	859.50	1115.33	1333.54	1046.62	1137.02
	742.54	842.11	1315.23	920.85	1026.95
	664.85	740.66	993.24	901.35	787.41
	552.21	697.78	728.59	617.68	634.40
	410.96	446.35	421.67	485.75	536.34
	398.20	377.18	361.71	417.39	473.40
	323.55	335.40	348.78	378.41	371.73
	281.31	280.37	342.15	330.35	314.49
	271.26	276.44	205.76	251.70	264.39
	222.53	186.10	163.07	212.51	236.41
	196.20	370.66 (i)	147.79	967.90 (i)	155.08
ZPE (eV)	0.70	0.73	0.98	0.75	0.91
TS (eV)	0.15	0.12	0.16	0.11	0.14
Rh ₂ @TiO ₂ (v)	(CO ₂ *) ₂ +2H*	T_S-4	HCOO*+H*	T_S-5	HCOOH*
Freq (cm ⁻¹)	2105.00	1828.08	2012.74	2580.65	3640.32
	1673.20	1602.16	1608.12	1309.02	2716.40
	1485.80	1473.09	1443.49	1194.47	1310.43
	1203.05	1225.79	1262.70	1168.44	1232.79
	1046.96	1133.81	1194.41	1042.15	1111.57
	755.26	968.23	1095.43	965.60	1040.66
	725.05	861.08	955.76	891.08	796.90
	653.55	708.93	697.13	630.82	612.91
	595.57	564.89	595.30	430.62	485.41
	483.53	373.68	371.17	410.44	384.31
	382.29	315.68	332.61	345.72	343.94
	317.40	279.79	300.21	332.65	301.76
	275.32	260.81	280.30	282.16	268.09
	265.66	178.43	259.10	190.98	239.80
	180.56	236.74 (i)	169.41	815.83 (i)	159.70
ZPE (eV)	0.75	0.73	0.78	0.73	0.91
TS (eV)	0.13	0.12	0.13	0.11	0.14

Table (S8) Calculated vibrational frequencies, zero point energies (ZPE) and entropy (TS) of different intermediates and transition states on supported tetramers for formic acid formation reaction, where the * denotes the adsorption site.

Ru ₄ @TiO ₂ (v)	(CO ₂ *) ₂ +2H*	T_S-4	HCOO*+H*	T_S-5	HCOOH*
Freq (cm ⁻¹)	1667.53	1830.11	2957.85	2956.98	3206.49
	1478.70	1644.45	1674.24	1687.89	2962.27
	1450.63	1184.79	1290.78	1255.76	1300.29
	1065.53	895.46	1140.17	995.81	1231.14
	847.14	859.86	1059.85	911.57	1158.03
	730.24	717.81	886.54	829.29	1007.85
	654.36	549.54	724.85	720.17	781.34
	588.83	501.05	607.38	533.03	671.54
	497.35	256.65	536.12	286.93	558.72
	406.74	231.61	406.42	235.45	535.66
	376.22	217.06	376.88	207.88	309.57
	297.07	168.22	323.85	178.10	281.39
	268.26	146.57	289.63	141.86	241.41
	239.80	136.29	254.93	139.92	216.57
	210.15	627.79 (i)	226.88	1168.72 (i)	197.17
ZPE (eV)	0.67	0.58	0.79	0.69	0.91
TS (eV)	0.14	0.20	0.13	0.19	0.14
Rh ₄ @TiO ₂ (v)	(CO ₂ *) ₂ +2H*	T_S-4	HCOO*+H*	T_S-5	HCOOH*
Freq (cm ⁻¹)	2079.71	1979.28	3002.58	2969.89	3375.94
	2056.68	1797.69	1298.71	1606.93	3000.69
	1433.79	1406.08	1221.57	1267.09	1288.66
	1167.01	1118.48	1189.46	1038.33	1212.45
	759.58	776.94	1075.20	935.95	1130.80
	716.90	743.51	937.74	780.34	975.27
	665.88	682.31	852.84	654.90	743.02
	591.04	619.84	629.75	484.37	572.98
	560.63	405.88	599.57	237.17	526.78
	400.36	334.78	531.81	221.35	486.30
	381.27	303.89	412.56	195.35	327.28
	331.71	250.78	335.31	145.56	288.58
	260.19	238.47	296.39	113.02	270.59
	239.00	200.43	280.12	100.96	218.02
	200.25	725.01 (i)	225.34	1359.42 (i)	207.70
ZPE (eV)	0.73	0.67	0.80	0.67	0.91
TS (eV)	0.14	0.14	0.12	0.22	0.14

Table (S9) Ratio of partition function of transition state to initial state (pre-reactive complex) of various surface reactions over unsupported ruthenium and rhodium clusters.

	Ru _x clusters					Rh _x clusters				
	Ru ₄	Ru ₅	Ru ₆	Ru ₇	Ru ₈	Rh ₄	Rh ₅	Rh ₆	Rh ₇	Rh ₈
$(\text{CO}_2^* + 2\text{H}^*)_1 \rightarrow \text{COOH}(\text{a})^* + \text{H}^*$	0.15	0.47	0.41	1.16	1.92	0.37	0.28	0.39	0.21	0.53
$\text{COOH}(\text{a})^* + \text{H}^* \rightarrow (\text{CO}_2^* + 2\text{H}^*)_1$	0.20	0.67	0.59	1.54	2.14	0.41	0.70	1.08	0.92	0.08
$\text{COOH}(\text{a})^* + \text{H}^* \rightarrow \text{COOH}(\text{s})^* + \text{H}^*$	0.93	0.44	1.16	1.09	1.10	1.06	1.67	1.18	1.02	1.76
$\text{COOH}(\text{s})^* + \text{H}^* \rightarrow \text{COOH}(\text{a})^* + \text{H}^*$	0.72	0.30	1.01	0.39	0.25	1.07	1.30	1.11	0.92	1.11
$\text{COOH}(\text{s})^* + \text{H}^* \rightarrow \text{CO}^* + \text{OH}^* + \text{H}^*$		1.87	3.05	1.25	0.18	0.57	1.40	3.79	5.70	0.22
$\text{CO}^* + \text{OH}^* + \text{H}^* \rightarrow \text{COOH}(\text{s})^* + \text{H}^*$		0.51	1.31	1.13	0.46	0.14	0.41	0.77	2.09	0.55
$\text{CO}^* + \text{OH}^* + \text{H}^* \rightarrow (\text{CO}^* + \text{H}_2\text{O}^*)_1$	0.30	1.15	1.12	0.25	1.95	0.25	1.19	1.75	4.21	0.69
$(\text{CO}^* + \text{H}_2\text{O}^*)_1 \rightarrow \text{CO}^* + \text{OH}^* + \text{H}^*$	0.05	0.07	0.14	0.02	0.31	0.09	0.05	0.14	0.21	0.25
$\text{COOH}(\text{s})^* + \text{H}^* \rightarrow \text{FA}^*$	0.54	0.45	1.16	0.12	0.08	0.31	0.43	0.69	0.88	0.02
$\text{FA}^* \rightarrow \text{COOH}(\text{s})^* + \text{H}^*$	1.00	0.47	1.40	0.71	0.39	0.81	0.91	0.71	0.58	0.08

Table (S10) Ratio of partition function of transition state to initial state (pre-reactive complex) of various surface reactions over supported ruthenium and rhodium clusters for RWGS reaction.

	Ru ₂ @TiO ₂ (v)	Rh ₂ @TiO ₂ (v)
$(\text{CO}_2^*)_1 + 2\text{H}^* \rightarrow \text{COOH}^* + \text{H}^*$	0.79	0.76
$\text{COOH}^* + \text{H}^* \rightarrow (\text{CO}_2^*)_1 + 2\text{H}^*$	0.78	0.85
$\text{COOH}^* + \text{H}^* \rightarrow \text{CO}^* + \text{OH}^* + \text{H}^*$	0.89	0.93
$\text{CO}^* + \text{OH}^* + \text{H}^* \rightarrow \text{COOH}^* + \text{H}^*$	0.27	0.26
$\text{CO}^* + \text{OH}^* + \text{H}^* \rightarrow \text{CO}^* + \text{H}_2\text{O}^*$	0.60	0.85
$\text{CO}^* + \text{H}_2\text{O}^* \rightarrow \text{CO}^* + \text{OH}^* + \text{H}^*$	0.02	0.66

Table (S11) Ratio of partition function of transition state to initial state (pre-reactive complex) of various surface reactions over supported ruthenium and rhodium clusters for formic acid formation reaction.

	Ru ₂ @TiO ₂ (v)	Rh ₂ @TiO ₂ (v)	Ru ₄ @TiO ₂ (v)	Rh ₄ @TiO ₂ (v)
$(\text{CO}_2^*)_2 + 2\text{H}^* \rightarrow \text{HCOO}^* + \text{H}^*$	0.62	0.90	4.03	1.02
$\text{HCOO}^* + \text{H}^* \rightarrow (\text{CO}_2^*)_2 + 2\text{H}^*$	0.45	0.77	4.98	1.51
$\text{HCOO}^* + \text{H}^* \rightarrow \text{HCOOH}^*$	0.37	0.67	4.29	11.13
$\text{HCOOH}^* \rightarrow \text{HCOO}^* + \text{H}^*$	0.60	0.58	3.23	7.21

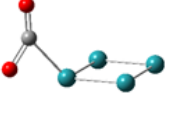
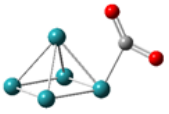
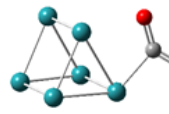
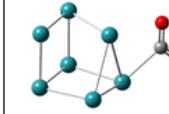
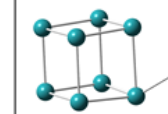
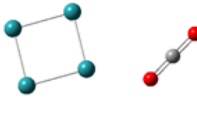
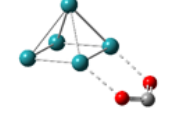
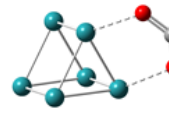
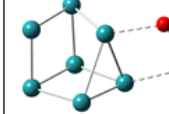
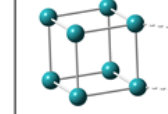
(CO ₂ *)-1					
ΔG_f	-0.04 (-0.39) ^a	-0.76 (-0.28) ^a	-0.63 (-0.19) ^a	-0.39 (-0.19) ^a	-0.34 (0.28) ^a
(CO ₂ *)-2					
ΔG_f	0.08 (-0.06) ^a	0.51 (0.84) ^a	0.23 (0.07) ^a	0.40 (0.11) ^a	0.29 (0.11) ^a

Figure (S1) Optimized geometries of CO₂ adsorbed ruthenium clusters. Free energy of CO₂ adsorption (ΔG_f) in eV unit. The values given in bracket corresponding to ΔG_f for rhodium clusters.

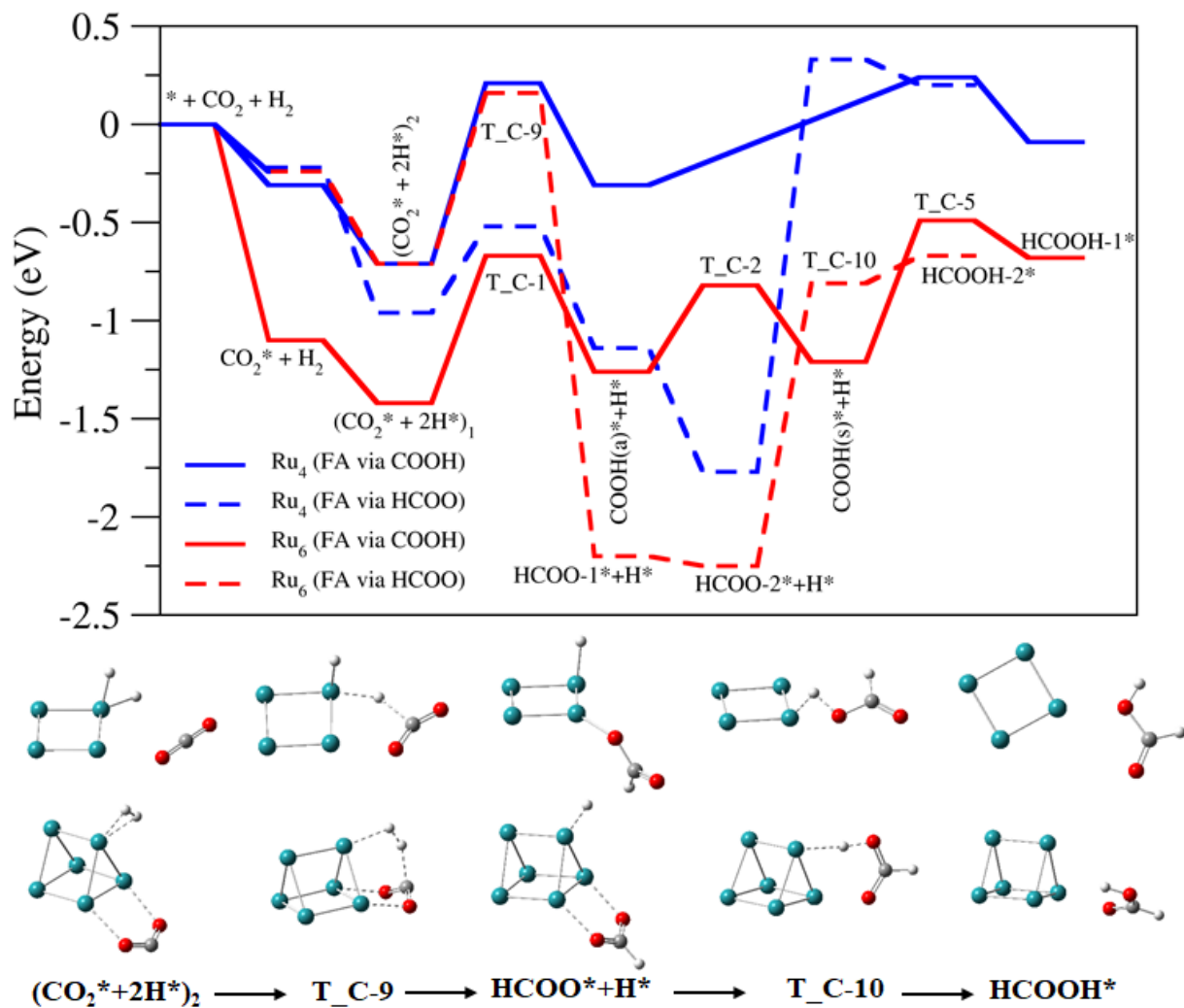


Figure (S2) Comparative energy diagrams of HCOOH formation through carboxyl (COOH*) and formate (HCOO*) intermediates on four and six membered ruthenium clusters (Ru₄ and Ru₆). Optimized geometries of intermediates and transition states have also been presented below.

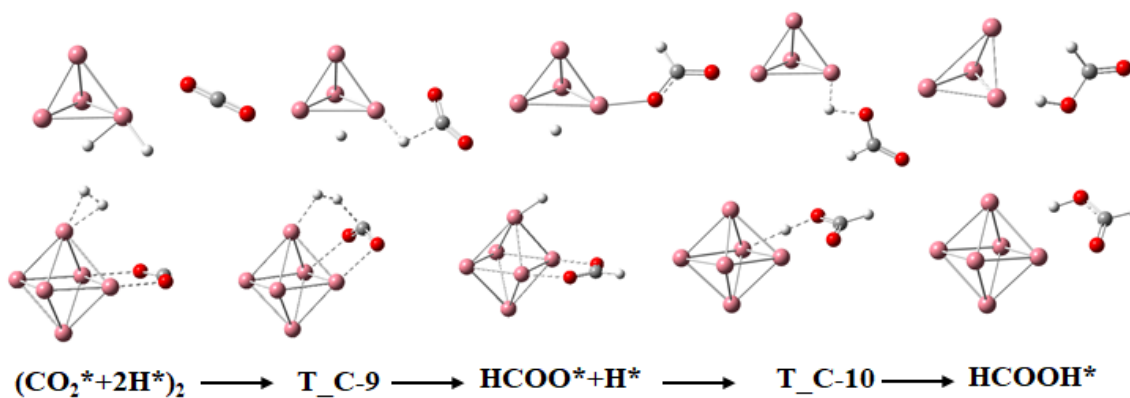
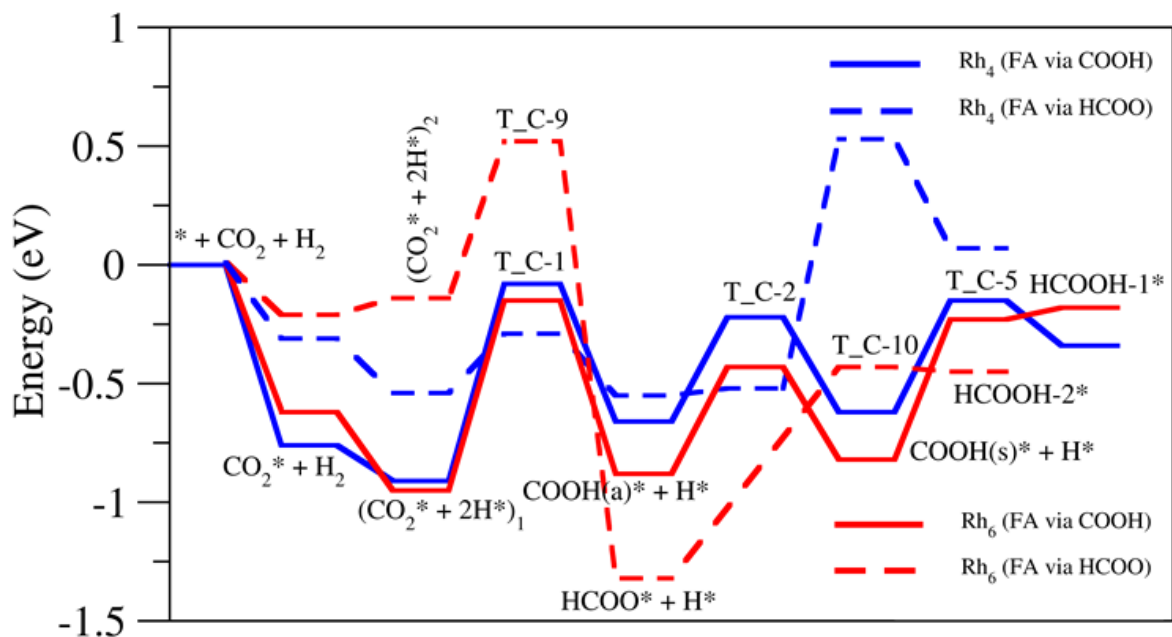


Figure (S3) Comparative energy diagrams of HCOOH formation through carboxyl (COOH*) and formate (HCOO*) intermediates on four and six membered rhodium clusters (Rh₄ and Rh₆). Optimized geometries of intermediates and transition states have also been presented below.

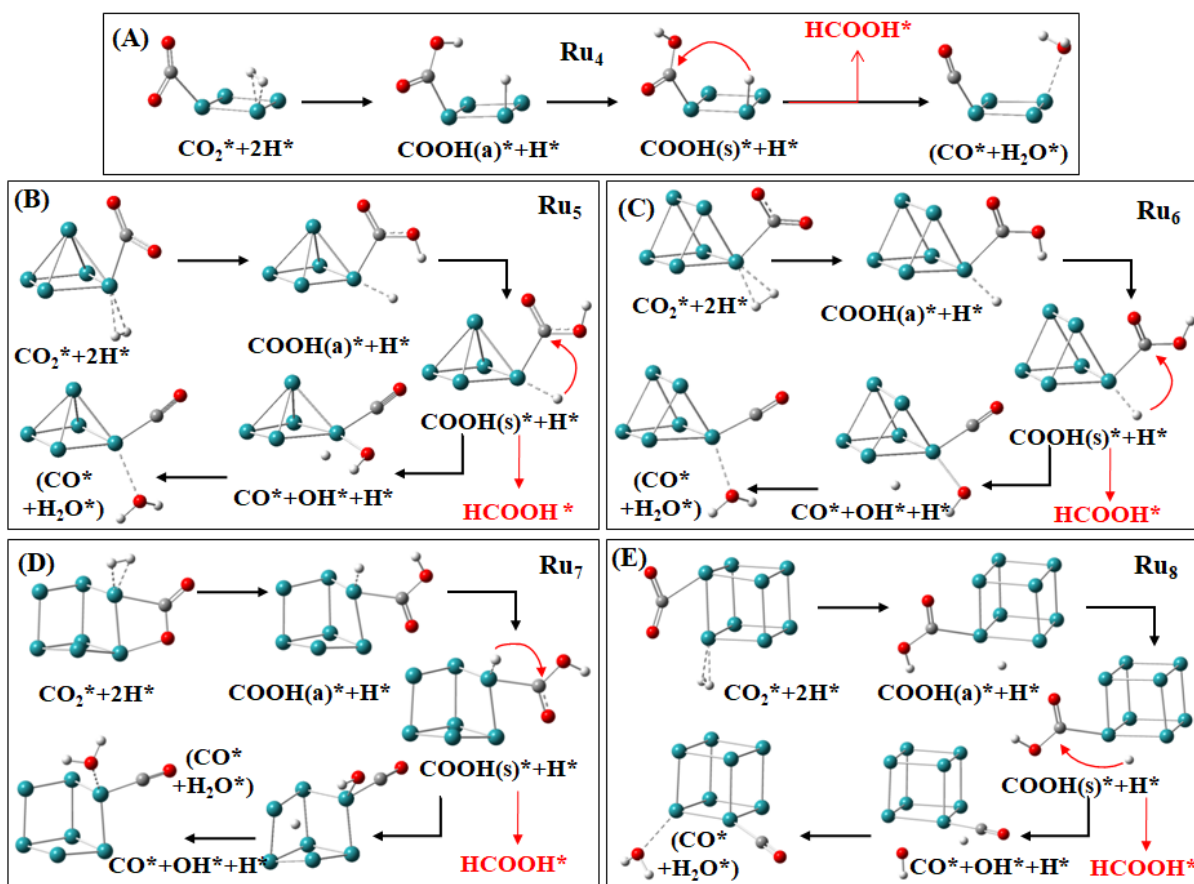


Figure (S4) CO_2 hydrogenation pathways on size selected subnanometer Ru_x clusters.

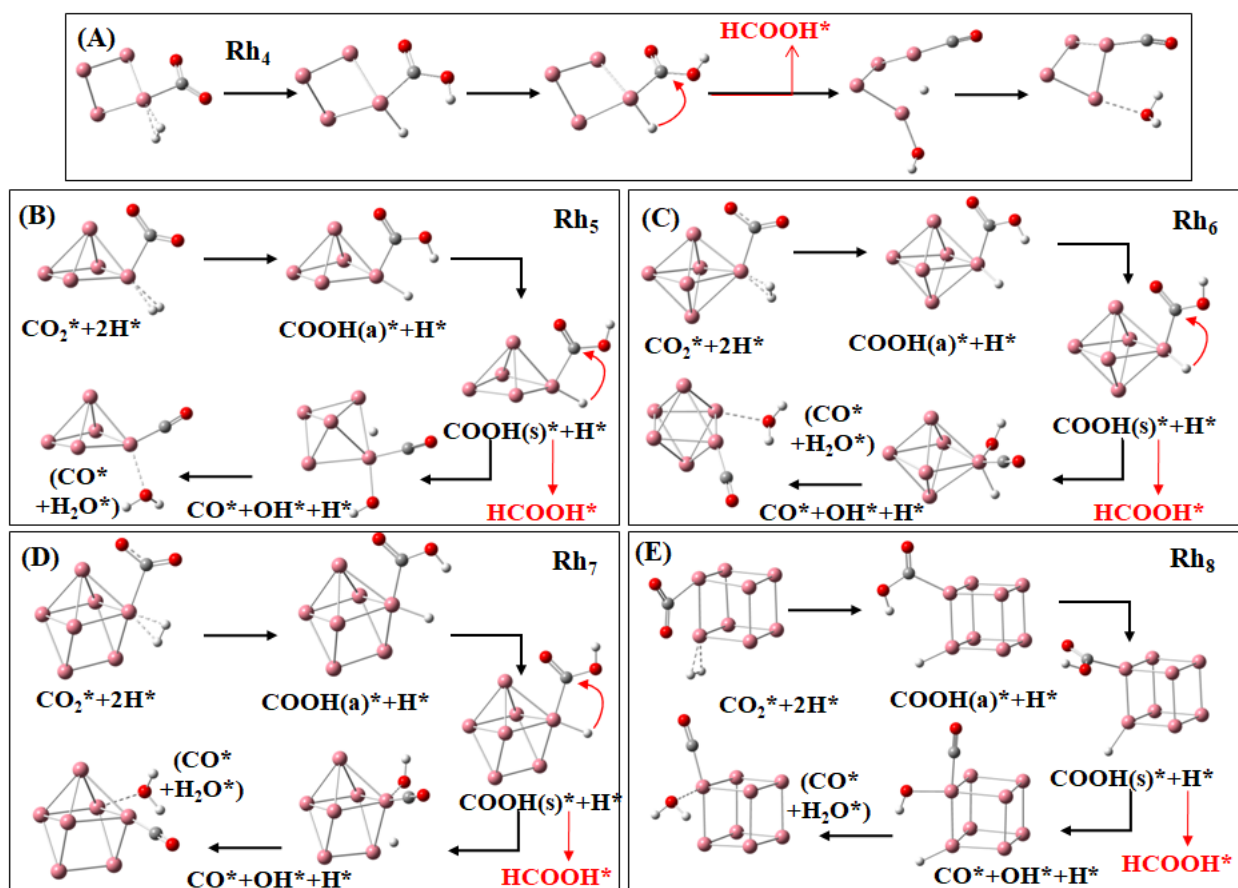


Figure (S5) CO₂ hydrogenation pathways on size selected subnanometer Rh_x clusters.

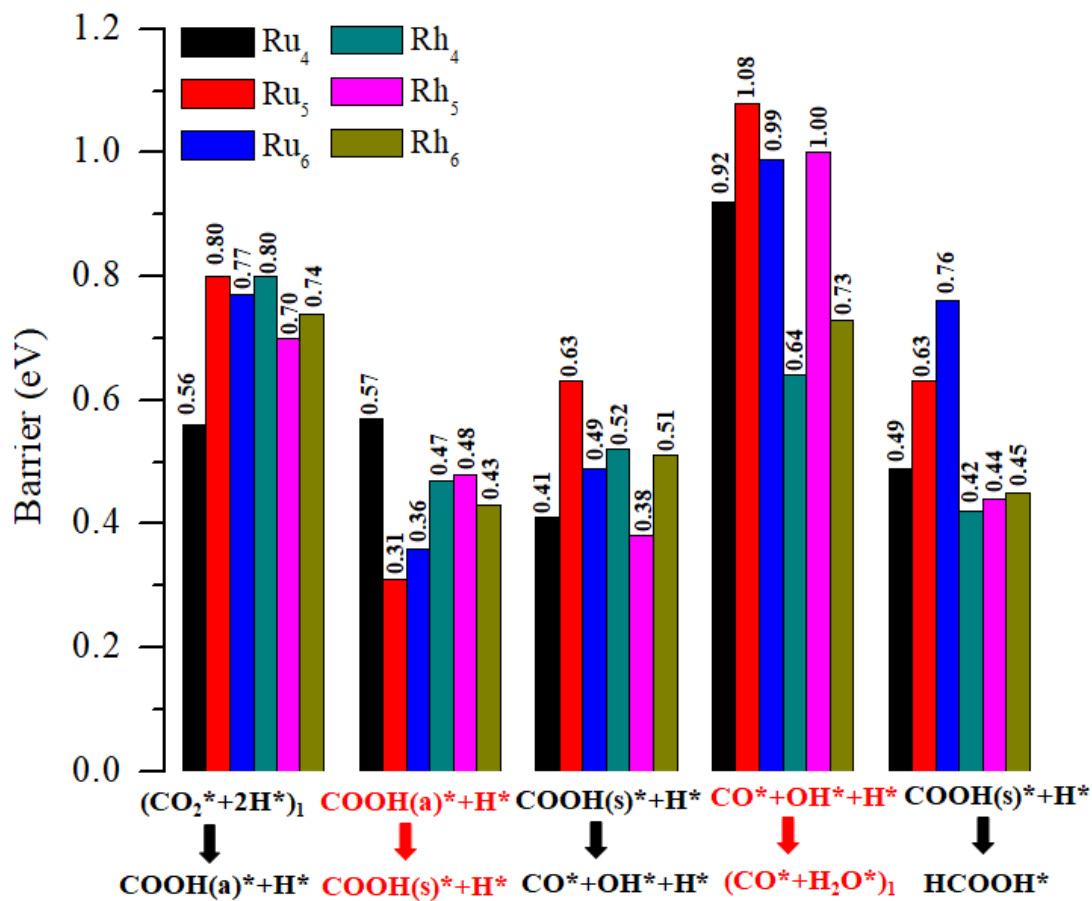


Figure (S6) Barrier heights (eV) of various elementary steps on selected subnanoclusters from B3LYP(D3)/def2-TZVP level of calculations.

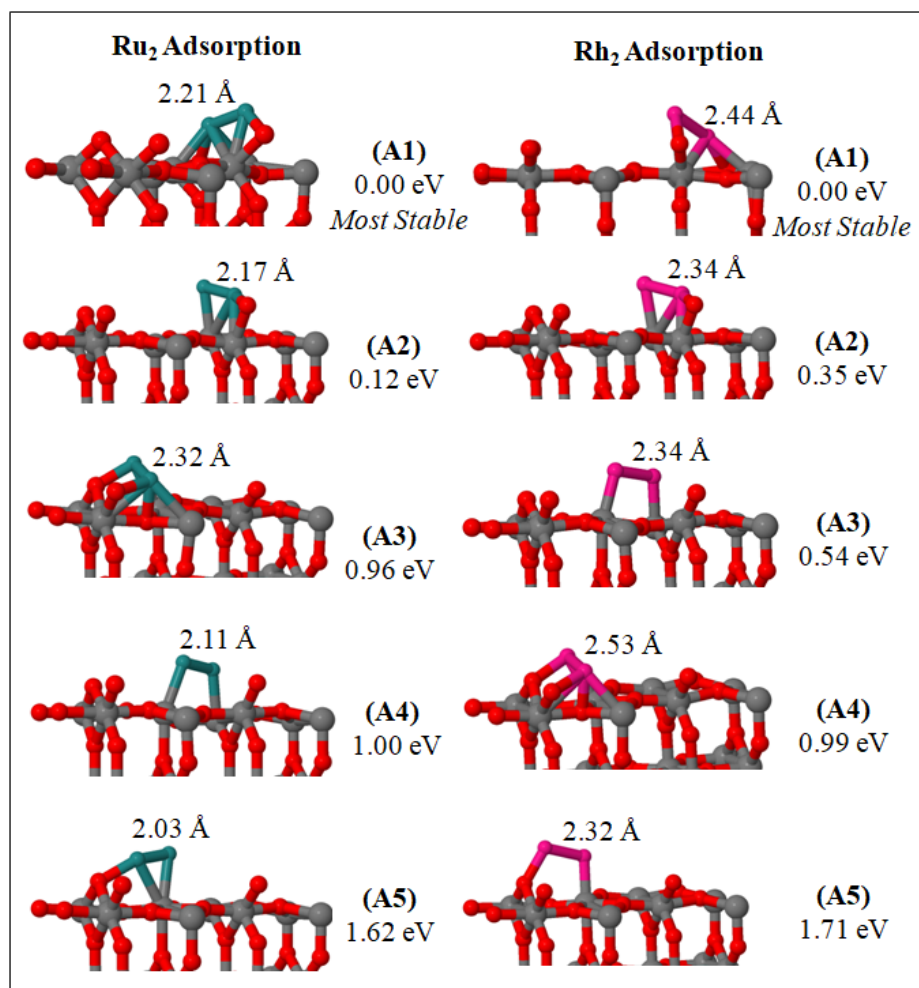


Figure (S7) Possible adsorption configurations of Ru₂ and Rh₂ dimers on oxygen defected TiO₂ support.

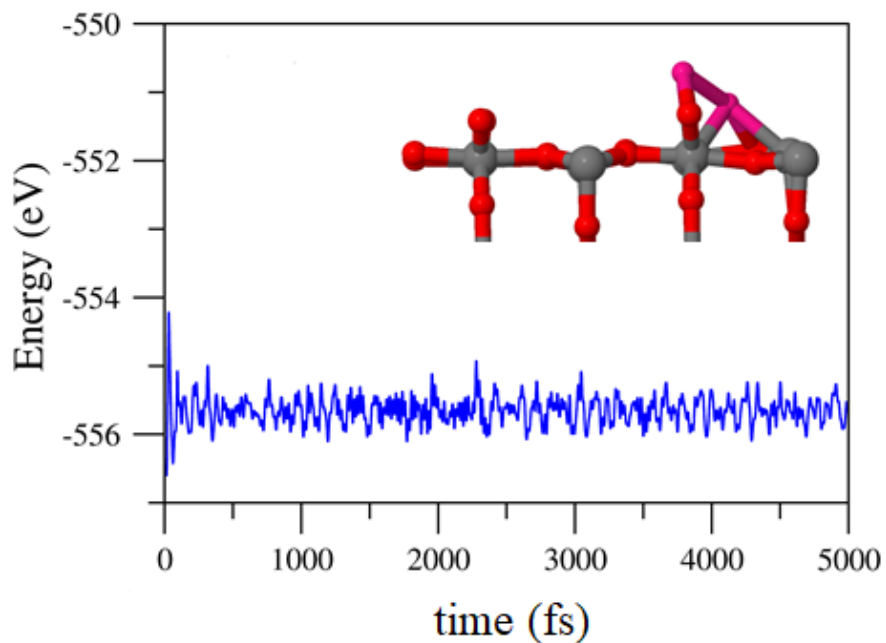


Figure (S8) Energy fluctuations of $\text{Rh}_2@ \text{TiO}_2(\text{v})$ vs time in AIMD simulations at 400 K.

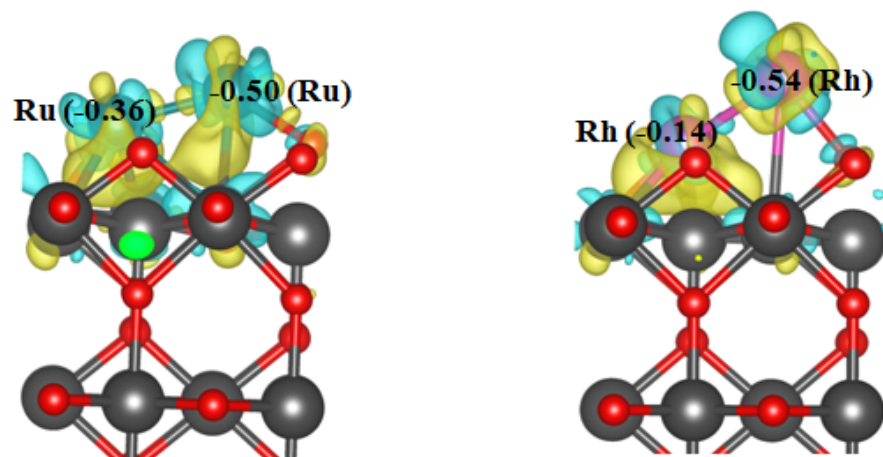


Figure (S9) Charge density difference plot of supported dimers. Charge depletion and accumulation are displayed in cyan and yellow, respectively. Negative sign indicates that electron flow from metal dimer to TiO_2 .

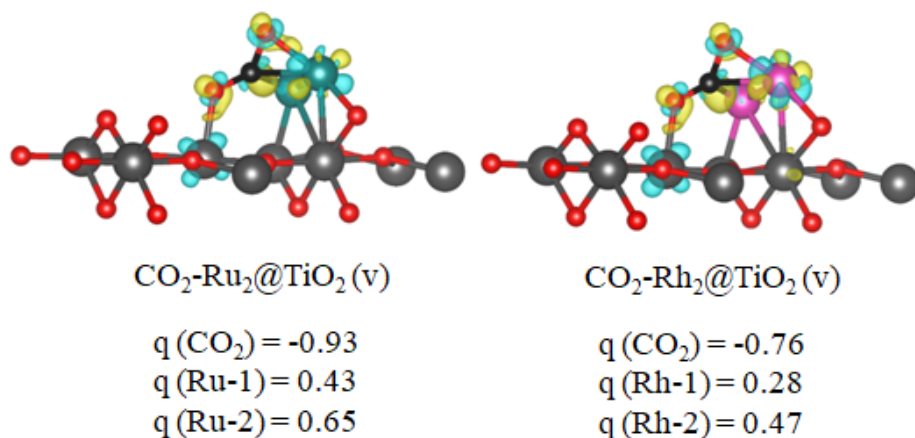


Figure (S10) Charge density difference plot and bader charges of CO_2 adsorbed supported dimers. Charge depletion and accumulation are displayed in cyan and yellow, respectively.

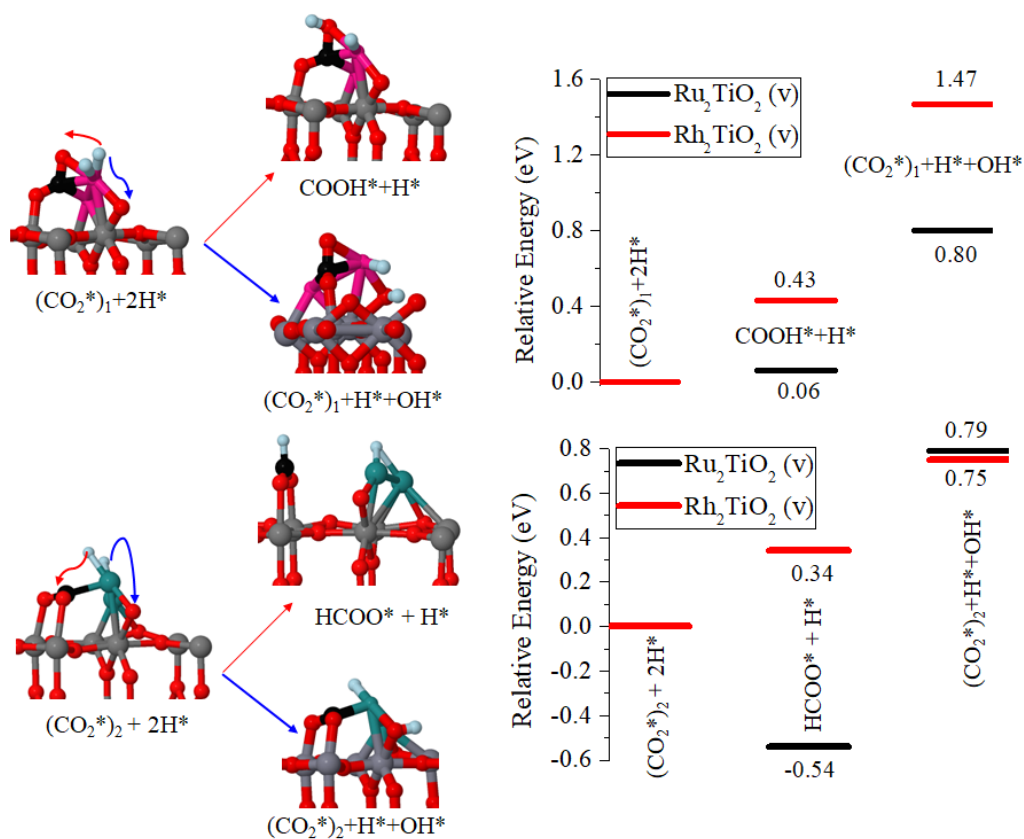


Figure (S11) Relative energies of various intermediates for the hydrogenation of O-atom of surface adsorbed CO_2^* and oxide surface.

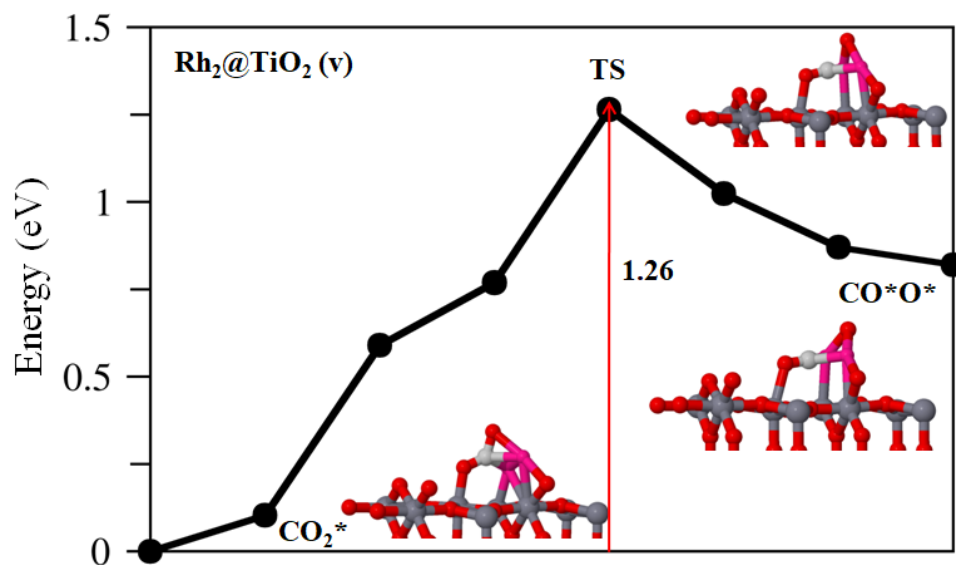


Figure (S12) Schematic energy profiles of CO₂ dissociation pathway over Rh₂@TiO₂(v) catalyst.

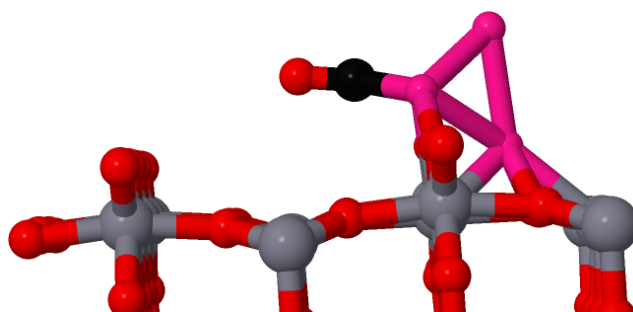


Figure (S13) Geometry of CO adsorbed TiO₂(v) supported Rh₄ cluster.

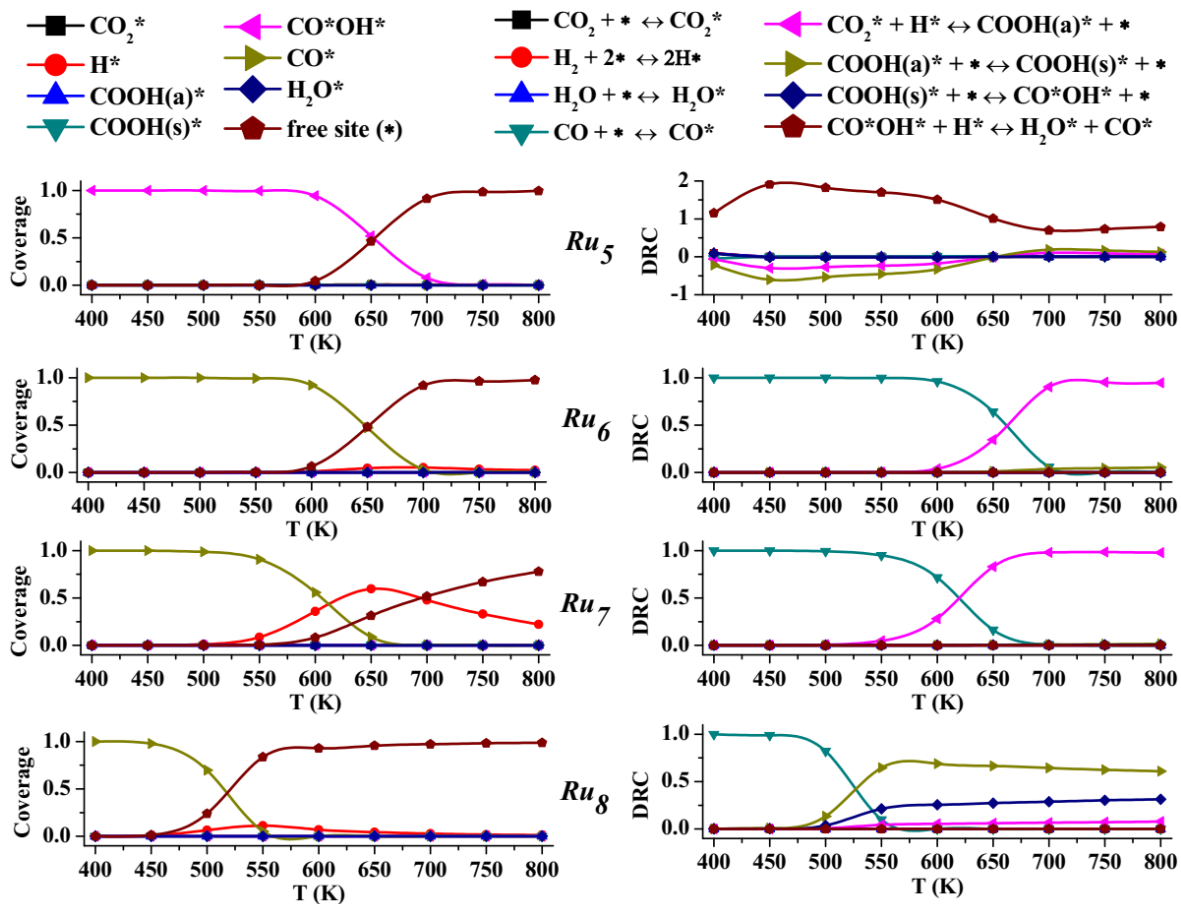


Figure (S14) Surface coverage and degree of rate control coefficient as function of temperature for unsupported Ru_x cluster catalyzed RWGS reaction.

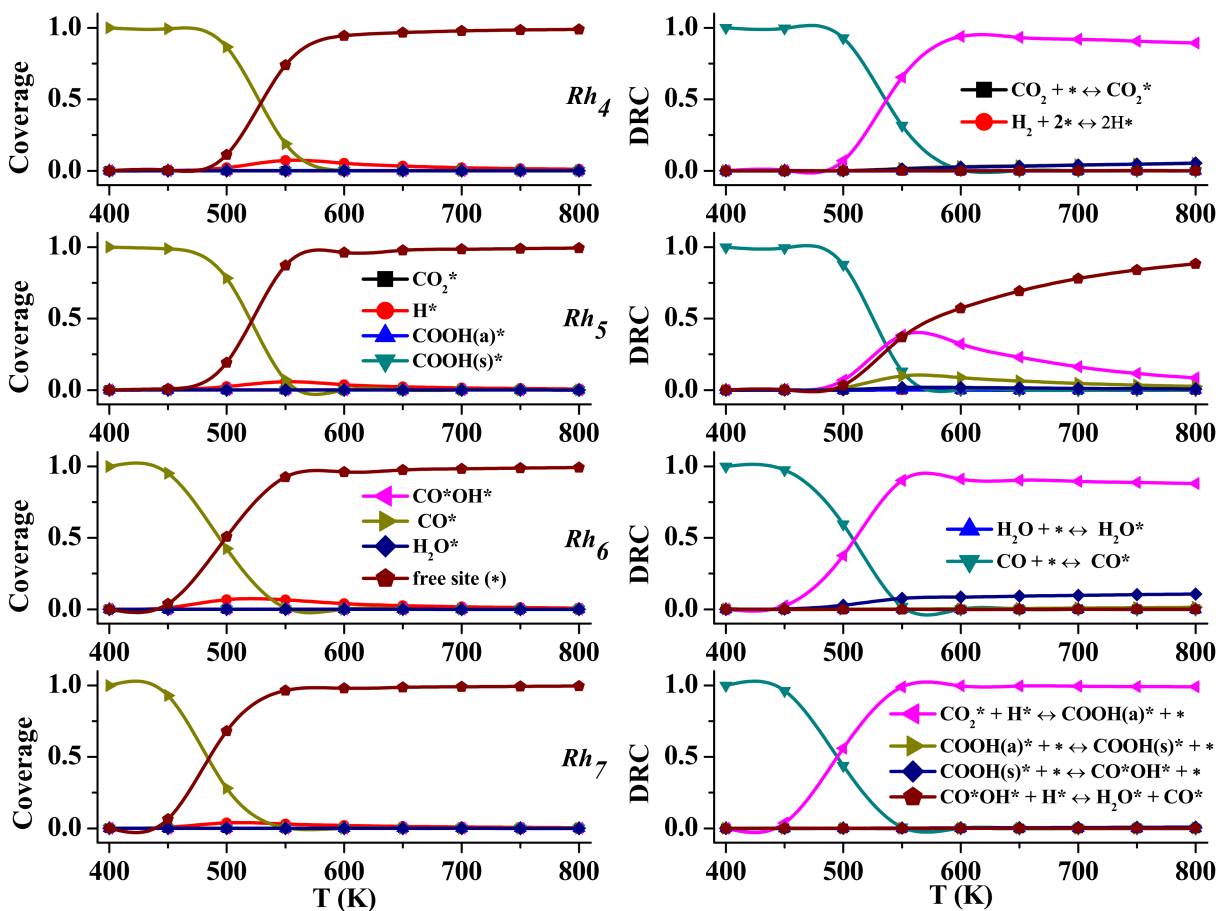


Figure (S15) Surface coverage and degree of rate control coefficient as function of temperature for unsupported Rh_x cluster catalyzed RWGS reaction.

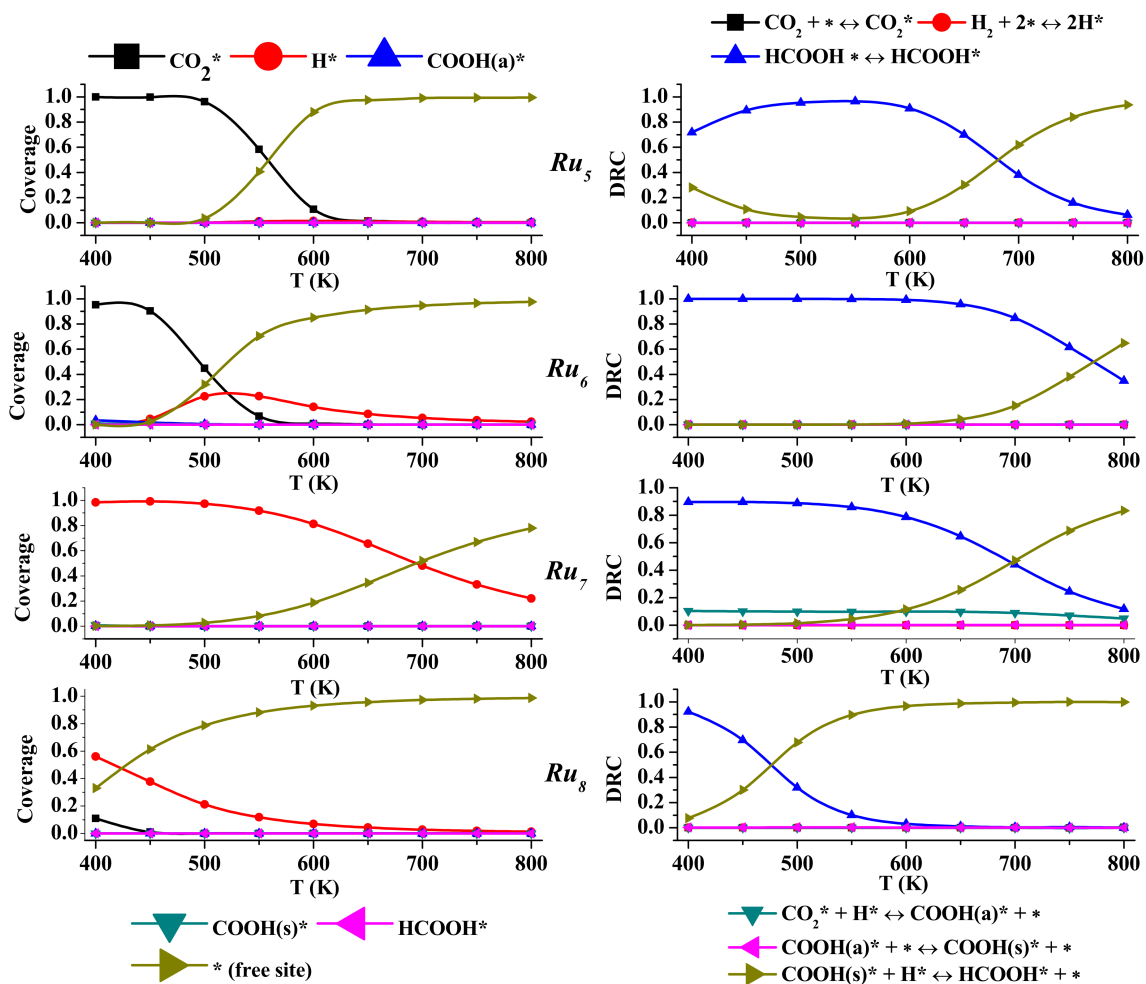


Figure (S16) Surface coverage and degree of rate control coefficient as function of temperature for unsupported Ru_x cluster catalyzed formic acid formation reaction.

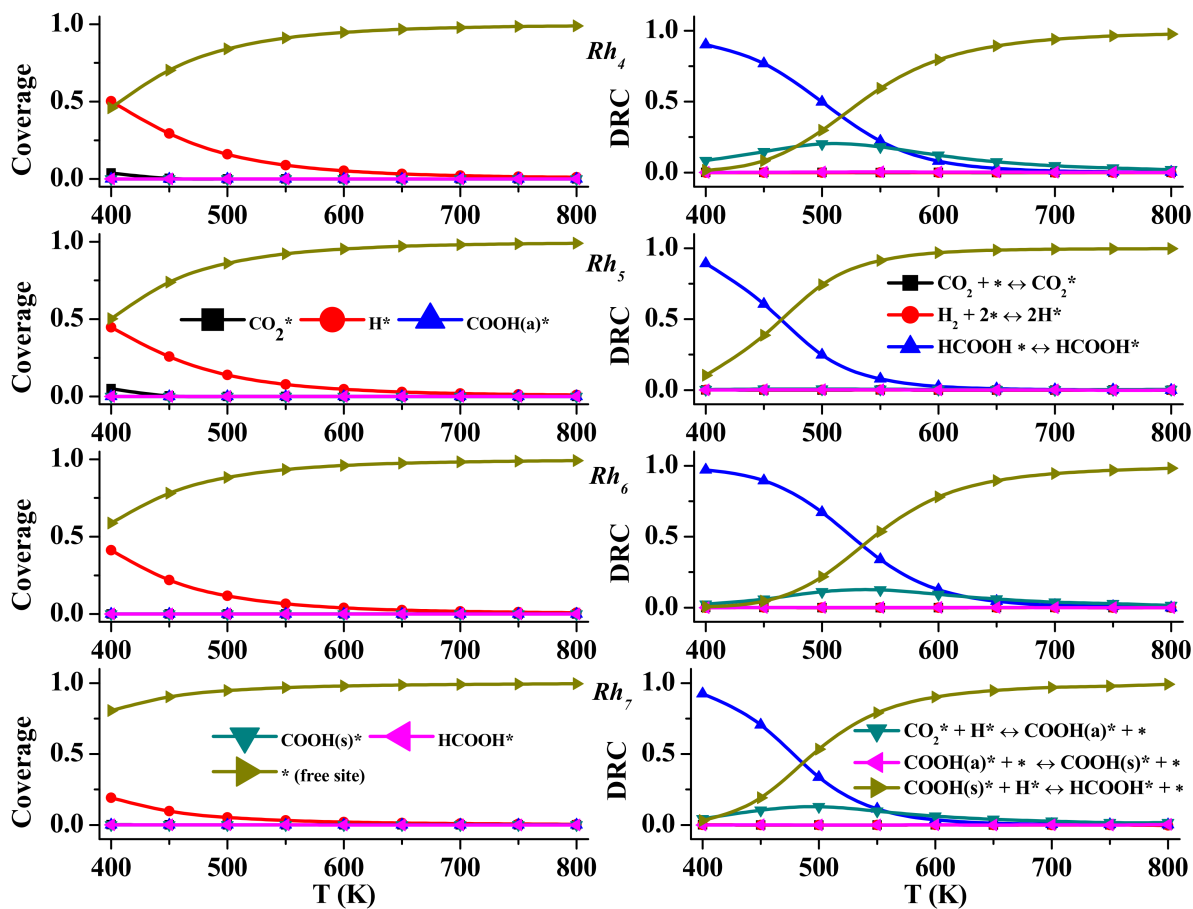


Figure (S17) Surface coverage and degree of rate control coefficient as function of temperature for unsupported Rh_x cluster catalyzed formic acid formation reaction.

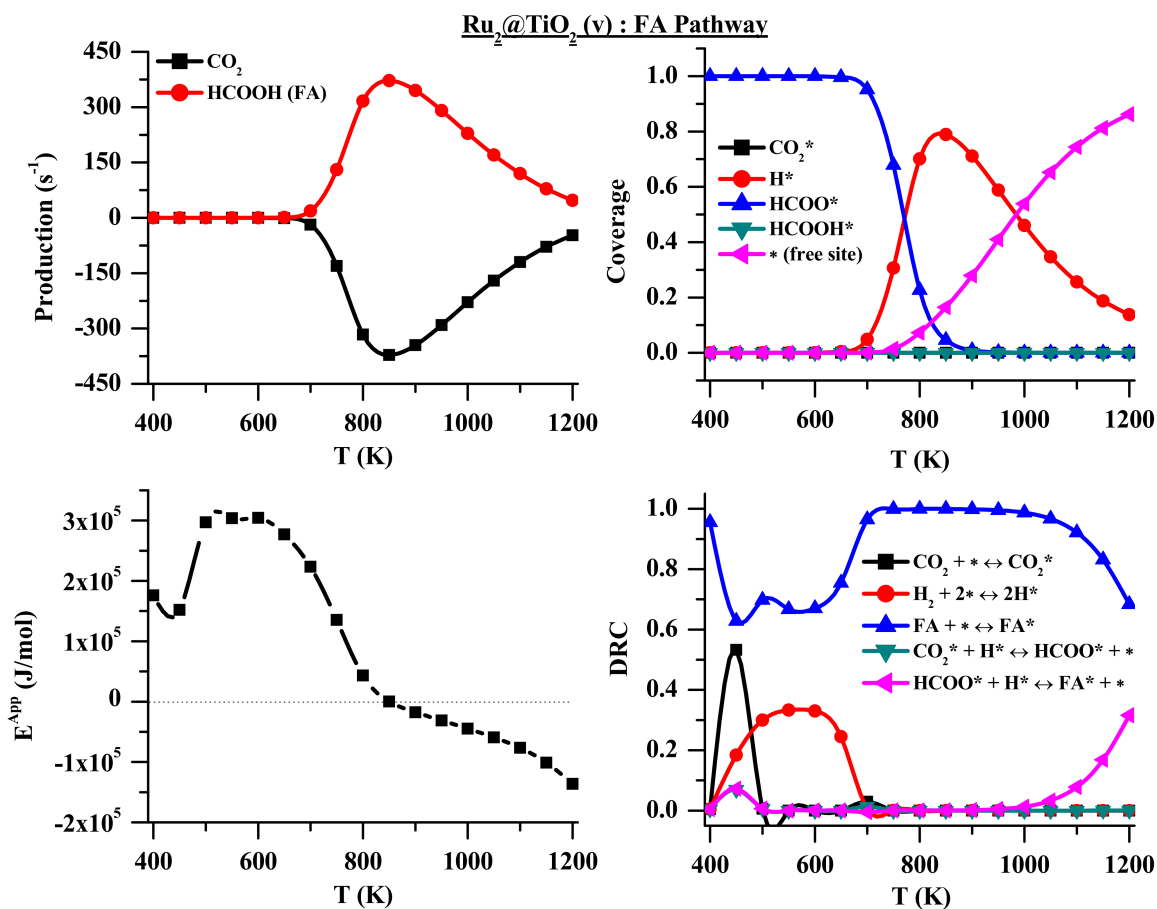


Figure (S18) Production rate, surface coverage, apparent activation barrier (E^{App}) and degree of rate control coefficient (DRC) as function of temperature for $\text{Ru}_2@\text{TiO}_2(\text{v})$ catalyzed FA formation reaction.

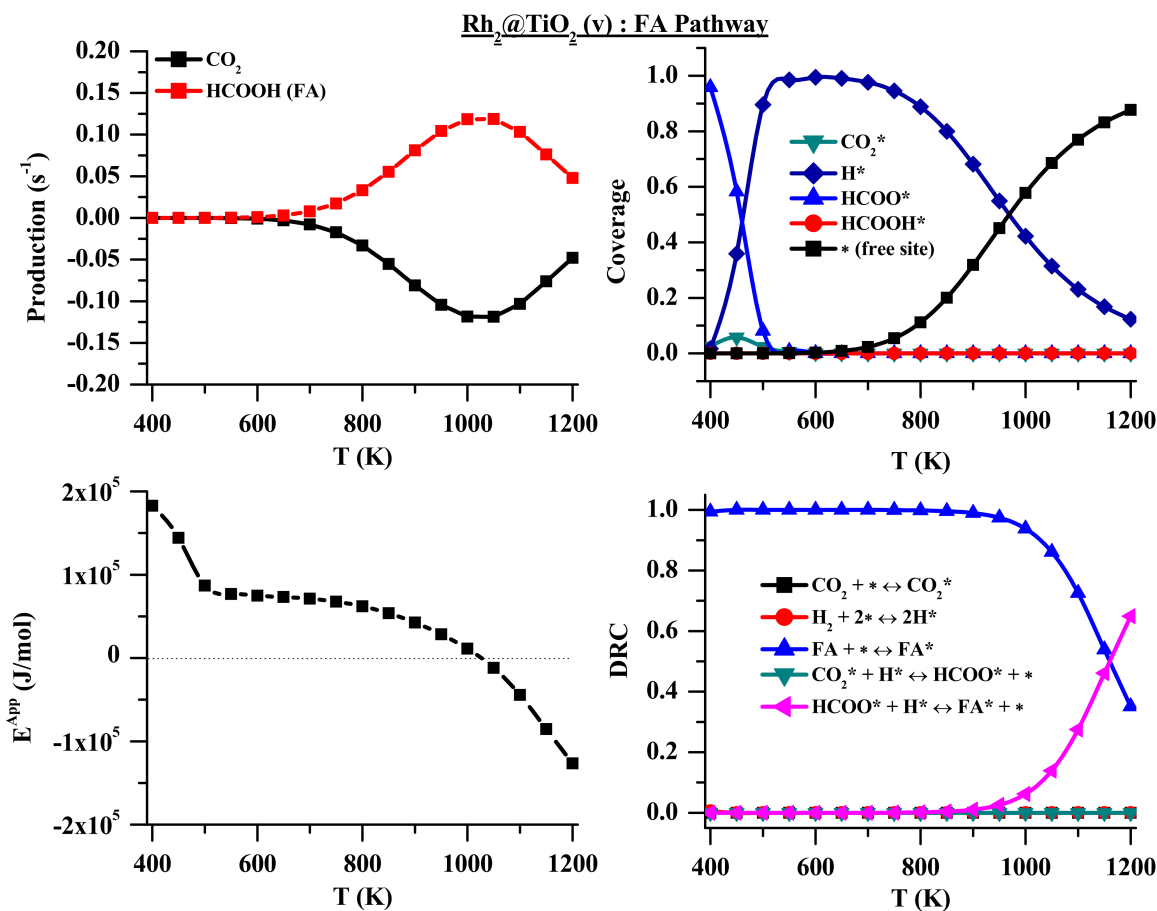


Figure (S19) Production rate, surface coverage, apparent activation barrier (E^{App}) and degree of rate control coefficient (DRC) as function of temperature for $\text{Rh}_2@\text{TiO}_2(\text{v})$ catalyzed FA formation reaction.

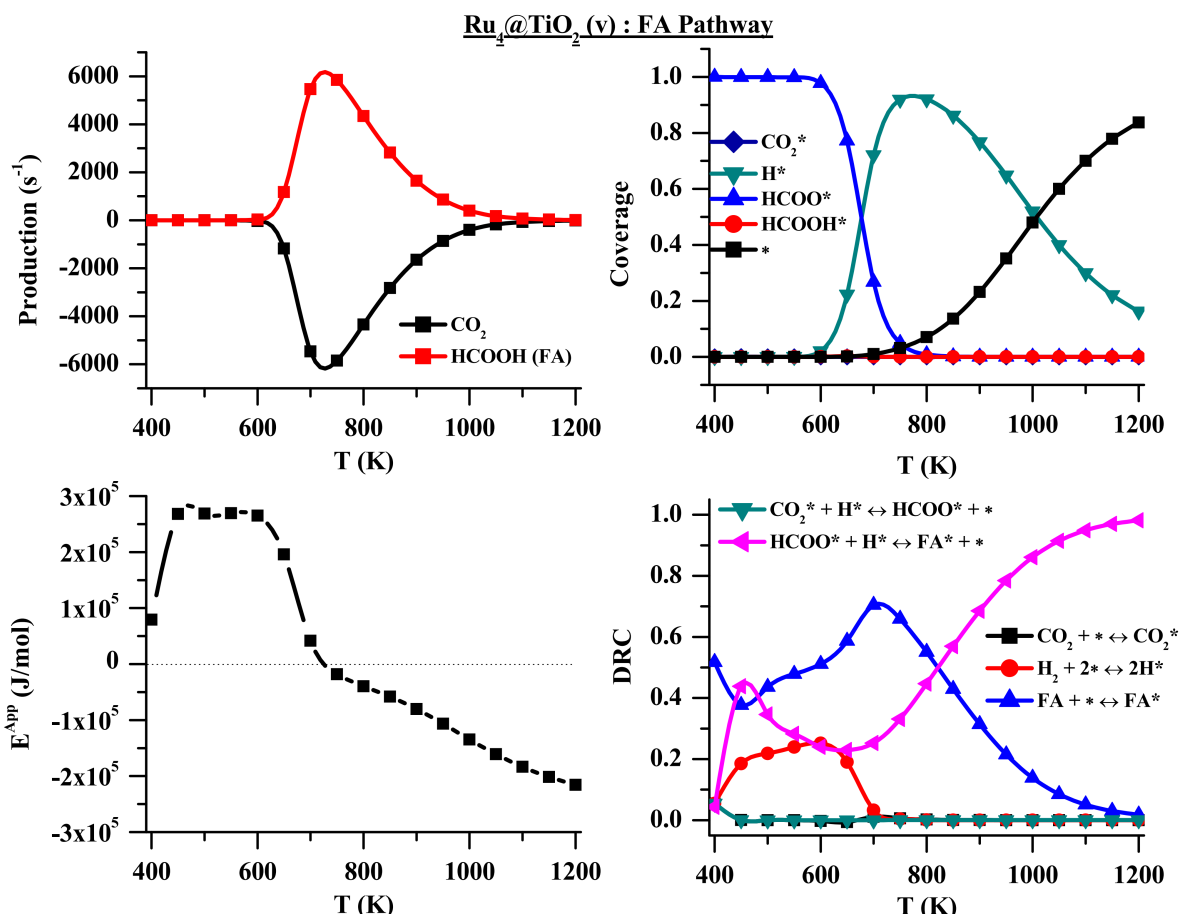


Figure (S20) Production rate, surface coverage, apparent activation barrier (E^{App}) and degree of rate control coefficient (DRC) as function of temperature for $\text{Ru}_4@\text{TiO}_2(\text{v})$ catalyzed formic acid formation reaction.

References

- (1) Pilot, I. A.; Van Santen, R. A.; Hensen, E. J. The optimally performing Fischer–Tropsch catalyst. *Angewandte Chemie* **2014**, *126*, 12960–12964.
- (2) Pilot, I. A.; Broos, R. J.; van Rijn, J. P.; van Heugten, G. J.; van Santen, R. A.; Hensen, E. J. First-principles-based microkinetics simulations of synthesis gas conversion on a stepped rhodium surface. *ACS Catalysis* **2015**, *5*, 5453–5467.
- (3) Liu, J.-X.; Richards, D.; Singh, N.; Goldsmith, B. R. Activity and selectivity trends in electrocatalytic nitrate reduction on transition metals. *ACS Catalysis* **2019**, *9*, 7052–7064.
- (4) Nitoń, P.; Żywociński, A.; Fiałkowski, M.; Hołyst, R. A "nano-windmill" driven by a flux of water vapour: a comparison to the rotating ATPase. *Nanoscale* **2013**, *5*, 9732–9738.
- (5) Eyring, H. The activated complex in chemical reactions. *The Journal of Chemical Physics* **1935**, *3*, 107–115.
- (6) Saputro, A. G.; Maulana, A. L.; Fathurrahman, F.; Shukri, G.; Mahyuddin, M. H.; Agusta, M. K.; Wungu, T. D. K.; Dipojono, H. K. Density functional and microkinetic study of CO₂ hydrogenation to methanol on subnanometer Pd cluster doped by transition metal (M= Cu, Ni, Pt, Rh). *International Journal of Hydrogen Energy* **2021**, *46*, 14418–14428.
- (7) Li, G.; Meeprasert, J.; Wang, J.; Li, C.; Pidko, E. A. CO₂ hydrogenation to methanol over Cd₄/TiO₂ catalyst: Insight into multifunctional interface. *ChemCatChem* **2022**, *14*, e202101646.
- (8) Spezzati, G. et al. CO oxidation by Pd supported on CeO₂ (100) and CeO₂ (111) facets. *Applied Catalysis B: Environmental* **2019**, *243*, 36–46.
- (9) Doherty, F.; Goldsmith, B. R. Rhodium Single-Atom Catalysts on Titania for Reverse Water Gas Shift Reaction Explored by First Principles Mechanistic Analysis and Compared to Nanoclusters. *ChemCatChem* **2021**, *13*, 3155–3164.

(10) Campbell, C. T. The degree of rate control: a powerful tool for catalysis research. 2017.